ACS OMEGA

http://pubs.acs.org/journal/acsodf

Article

Growth Kinetics of *Bacillus pasteurii* in Solid-Free Drilling Fluids

Zhijun Li,* Gan Zhao, Junxiu Chen, Kuo Liu, Haotian Xiang, and Yu Tian

Cite This: *ACS Omega* 2021, 6, 25170−25178

Read Online

ACCESS | Metrics & More | Article Recommendations

ABSTRACT: A broken stratum is a complex stratum often encountered during drilling. Under erosion of the drilling fluid and disturbance of the drill pipe string, the rock in the well wall of the broken stratum is prone to collapsing and falling off, causing the well wall to lose its stability. Improving the cementing force between the broken blocks and forming a complete well wall are essential for overcoming this instability. The present study combined microbially induced calcite precipitation technology with solid-free drilling fluid technology for the first time to formulate a drilling fluid to overcome the instability of the well wall of a broken stratum. However, first and foremost, the growth of microorganisms in drilling fluids must be elucidated. To this end, experimental and theoretical analyses were performed to examine *Bacillus pasteurii* growth in drilling fluids composed of a single agent or combinations of various materials, such as a zwitterionic coating agent (FA367), a biopolymer (XC), a polyacrylate polymer (PAC-LV), and potassium polyacrylate (K-PAM). Experimental *B. pasteurii* growth data were then fitted using a modified Gompertz model. The mean square error indicated that the generated model had a reasonable degree of fit, and the bias and accuracy factors showed that the model could predict *B. pasteurii* growth. Among the different drilling fluid combinations used, suitable fluids for *B. pasteurii* growth were XC alone, XC, and PAC-LV in the two-material-based fluid and FA367, XC, and K-PAM in the three-material-based fluid. These results provide a solid foundation for the development of microbial drilling fluids to solve instability problems in broken geological formations.

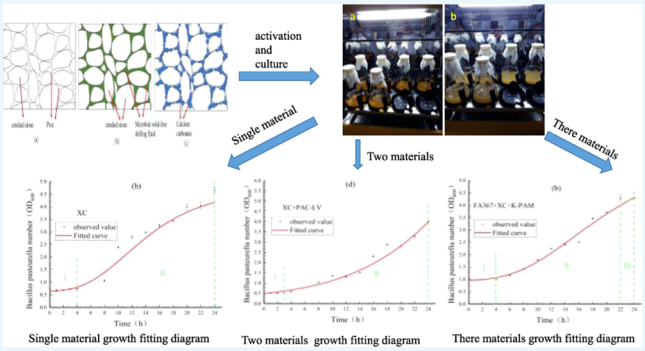

INTRODUCTION

The term "geological core drilling" refers to a geological project that uses certain drilling machinery and technology to obtain rock cores below the surface to evaluate geological and mineral resource parameters.[1] During geological core drilling, rock masses with a broken mechanical behavior under external forces, also referred to as broken formations, are often encountered reliably. The most common broken geological formations include coal seams, shale layers, limestone, and dolomites.[2] These formations have remarkable features, including being broken and incomplete, having poor cementation, developing fractures, and low formation strength.[3] Drilling involves cutting the rock by rotating a drill bit to form a hole of a specific diameter.[4] The drilling fluid then enters the bottom of the hole through the drill pipe string and returns to the hole through the annular gap between the drill pipe and borehole wall. During the entire circulation of the drilling fluid, it enters the rock surrounding the borehole wall through cracks, fluid seepage, and chemical action, and the stone cohesion and internal friction angle are reduced, causing the cracks to gradually expand and penetrate, resulting in the rupture of the surrounding rock of the borehole wall, making it unstable.[5,6] Improving the cementing force between the broken blocks by rapidly plugging the cracks and forming a complete shaft wall is essential for enhancing the stability of broken shaft walls. The most commonly used technique for plugging geological fractures and preventing the drilling fluid or filtrate from entering geological formations through fractures is adding various types of plugging agents to the drilling fluid;[7−9] however, this technology does not entirely solve the shaft wall instability in broken formations. Thus, there is an urgent need to develop other methods to solve this problem. Microbiologists use specific microorganisms, including urease-producing and denitrifying bacteria, to rapidly precipitate calcite−calcium carbonate crystals with excellent cementation by providing the microorganisms with abundant calcium ions (Ca^{2+}) and nitrogen. The mineralization effect of these microbes is known as microbially induced calcite precipitation (MICP) technology[10] and was first applied to plug porous medium materials.[11,12] Subsequently, the use of MICP has become widespread, and MICP has been used to repair surface

Received: May 19, 2021
Accepted: September 13, 2021
Published: September 27, 2021

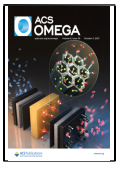

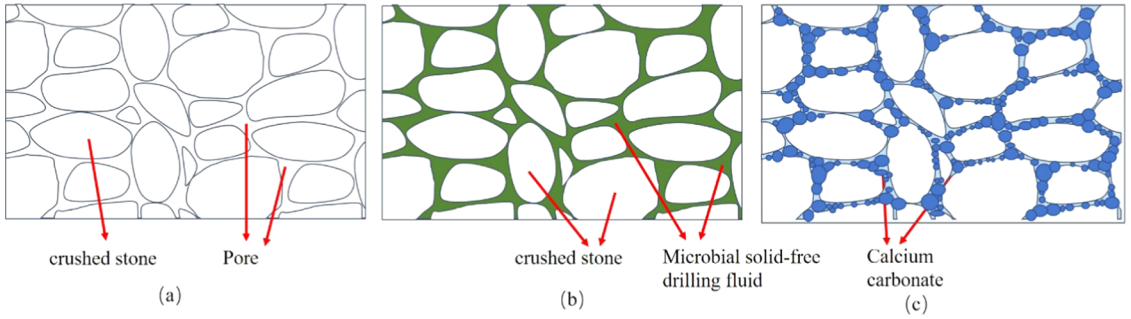

Figure 1. Schematic diagram of a microbial-cemented crushed stone: (a) broken stratum, (b) microbial solid-free drilling fluid acting on the broken stratum, and (c) broken stratum after cementation.

cracks in stone- and cement-based materials.[13,14] Many studies have been conducted on soil reinforcement.[15−18] The available MICP methods are urea hydrolysis, denitrification, ferric iron reduction, and sulfate reduction. Urea hydrolysis is simple and easy to control and can quickly produce large amounts of CO_3^{2-}. Therefore, urea hydrolysis-based MICP has been widely used as the mainstream calcium carbonate biomineralization technique.[19,20] Most urea hydrolysis-based MICP methods have utilized high-yield urease-producing *Bacillus pasteurii*, which has strong environmental adaptability. In these methods, urea is used as an energy source to produce a large amount of highly active urease via metabolism by *B. pasteurii*, wherein urea is hydrolyzed into NH_4^+ and CO_3^{2-}. CO_3^{2-} reacts with Ca^{2+} from the environment, and calcium carbonate crystals are precipitated around *B. pasteurii*.[21] Figure 1 shows a schematic of a microbial-cemented crushed stone.

$$Ca^{2+} + \text{cell} \rightarrow \text{cell} - Ca^{2+}$$

$$NH_2 - CO - NH_2 + 2H_2O \xrightarrow{\text{bacteria}} 2NH_4^+ + CO_3^{2-}$$

$$CO_3^{2-} + \text{cell} - Ca^{2+} \rightarrow \text{cell} - CaCO_3\downarrow$$

Microbially induced carbonate precipitation (MICP) provides a potential solution for the instability of fractured geological formations during core drilling. If MICP can be integrated into drilling fluids, the use of microorganisms to induce the formation of calcium carbonate crystals may fill the fractures and fissures of broken geological formations and cement and improve the mechanical strength and stability of broken geological formations; however, the drilling fluid is a complex dispersion system composed of various materials. The key to the successful application of MICP is whether microorganisms can grow normally in the drilling fluid. At present, research on microbial growth kinetics has mainly focused on environmental monitoring, food safety, and clinical analysis.[22] The growth kinetics of microorganisms in drilling fluids has not yet been studied. Many microorganisms can precipitate calcium carbonate;[23] however, not all are suitable for use in drilling fluids. *B. pasteurii* is a nonpathogenic, aerobic Gram-positive bacterium isolated from the soil with strong viability.[24]

In the present study, *B. pasteurii* growth in drilling fluids containing a zwitterionic coating agent (FA367), a biopolymer (XC), a polyacrylate polymer (PAC-LV), and potassium polyacrylate (K-PAM) was tested and analyzed. We aimed to establish a foundation for developing a microbial drilling fluid to effectively solve structural instability in broken geological formations.

RESULTS AND DISCUSSION

***B. pasteurii* Growth in a Liquid Medium.** The growth curve of *B. pasteurii* in a liquid medium is shown in Figure 2.

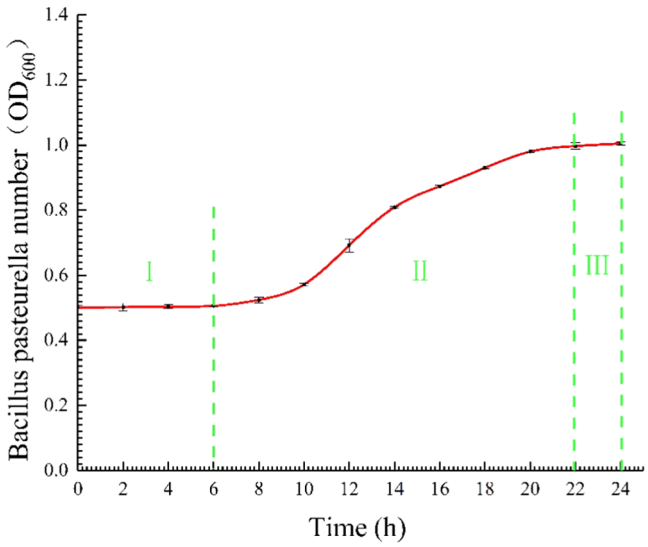

Figure 2. Growth kinetics of *B. pasteurii* in a liquid medium.

The growth curve of *B. pasteurii* in the liquid medium was an "S" shape. In Figure 2, parts I, II, and III represent the three periods of *B. pasteurii* growth, namely, the lag, logarithmic, and stationary phases, respectively. During the lag phase, the bacterial body became enlarged and bacterial metabolism was activated. It synthesized and accumulated sufficient enzymes, coenzymes, and intermediate metabolites for the division and reproduction of bacteria in the process of metabolism. During the logarithmic phase, the bacterial growth rate was the highest, the components of each part of the bacteria were uniform, the enzyme system was active, metabolism was healthy, and the microbial cells had the strongest ability to resist adverse environments. During the stationary phase, the growth rate stopped or approached zero; this implied that the number of new and dead cells was in a dynamic balance, the number of viable cells remained relatively stable and reached the highest level, the yield of bacteria reached the highest level, and the speed of cell division decreased. *B. pasteurii* had a growth lag phase of 0−6 h, the OD_{600} value was 0.48 at 6 h, the growth phase was logarithmic and occurred within 6−22.5 h, the OD_{600} value was 1.1 at 22.5 h, and the steady growth phase occurred from 22.5 to 24 h.

https://doi.org/10.1021/acsomega.1c02616
ACS Omega 2021, 6, 25170−25178

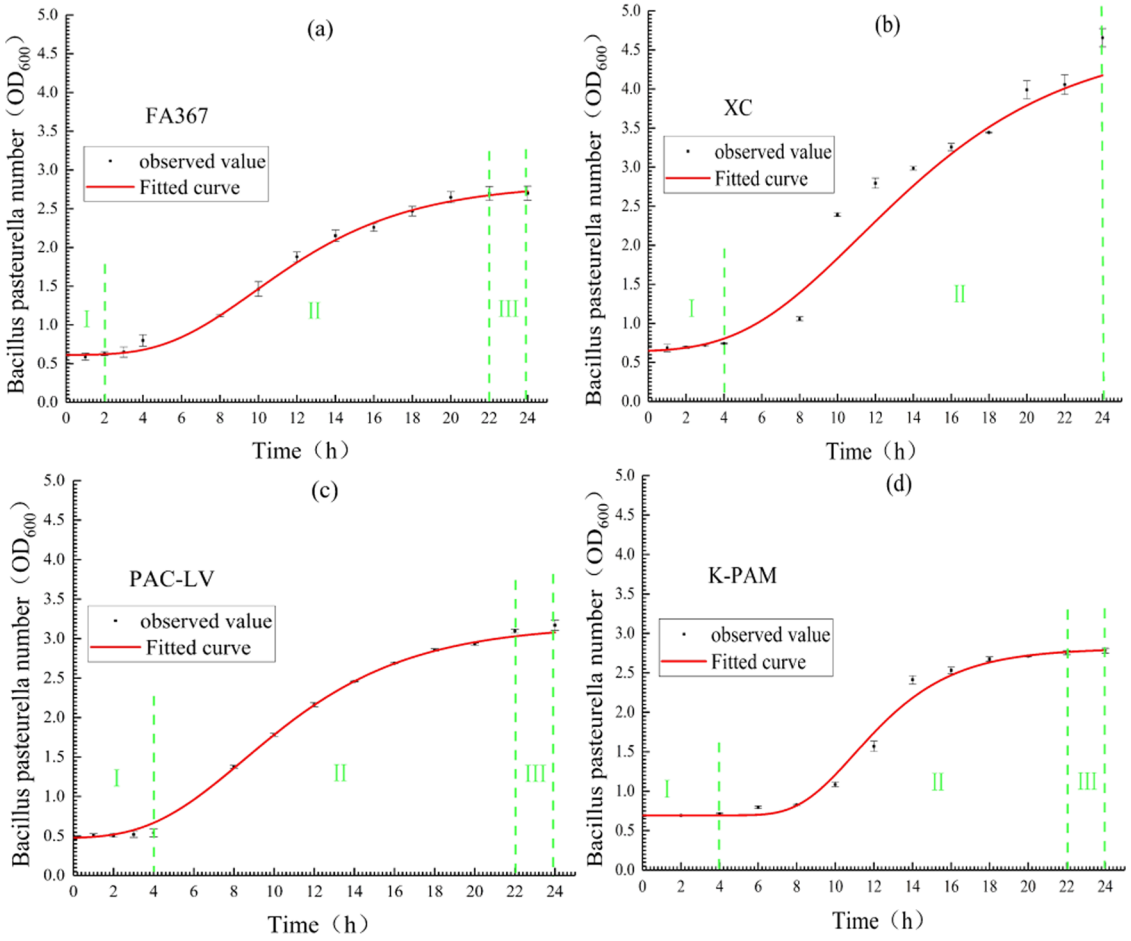

Figure 3. Growth curve of *B. pasteurii* in the drilling fluid containing (a) FA367, (b) XC, (c) PAC-LV, and (d) K-PAM.

Growth Kinetics of *B. pasteurii* in a Single-Material Solid-Free Drilling Fluid. The growth kinetics of *B. pasteurii* in a single-material drilling fluid is shown in Figure 3. In the FA367 solid-free drilling fluid, the growth lag period of *B. pasteurii* was 2 h, whereas in the other three solid-free drilling fluids, the growth lag period was 4 h. Within 24 h, *B. pasteurii* was still in the logarithmic growth phase in the XC solid-free drilling fluid (Figure 3b). In contrast, its growth plateaued in the other three solid-free drilling fluids within the same period. In the FA367 and XC solid-free drilling fluids, the logarithmic growth period of *B. pasteurii* was 20 h, while it was 18 h for other fluids.

Overall, *B. pasteurii* growth in the XC solid-free drilling fluid was the best, with an OD_{600} value of 4.7 at 24 h (Figure 3b), whereas the growth in the K-PAM solid-free drilling fluid was the worst within 24 h, with a maximum OD_{600} value of 2.6 (Figure 3d); in addition, the growth rate was slow during the logarithmic growth period. This is because XC is a composite polysaccharide,[25] providing an additional carbon source that is beneficial for *B. pasteurii* growth. In addition, K-PAM is a polymer of acrylic acid, and the pH of its solution is relatively acidic, which is not suitable for *B. pasteurii* growth. In the FA367 and PAC-LV solid-free drilling fluids, *B. pasteurii* grew suitably within 24 h, and the maximum OD_{600} values observed were 2.8 and 3.3, respectively (Figure 3a,b). Growth rates of *B. pasteurii* from the observed OD_{600} values in Figure 3a–d were 8.875, 16.733, 11.125, and 8.75%, respectively.

Among the four single-material drilling fluids, the growth fitting curves of *B. pasteurii* were all the typical S type, conforming to the characteristics of the used model. The model fit and verification parameters are presented in Table 1.

Table 1. Model Fit and Verification Parameters (Drilling Fluid Composed of a Single Material)

drilling fluid composition	MSE	B_f	A_f
FA367	0.00335	0.99112	1.03221
XC	0.07327	1.00951	1.08741
PAC-LV	0.00343	1.01333	1.03642
K-PAM	0.01123	0.99519	1.03994

As shown in Table 1, the mean square error (MSE) after fitting the solid-free drilling fluid comprising four single materials was less than 0.1, indicating that the model had a reasonable fit. The bias factor (B_f) value in the XC solid-free drilling fluid approached 1, and the accuracy factor (A_f) in the FA367 solid-free drilling fluid was the closest to 1. In general, B_f and A_f in each solid-free drilling fluid were close to 1.

In summary, the XC solid-free drilling fluid had a short lag time, a higher number of bacteria, and the fastest growth rate among all drilling fluids tested; therefore, it would be better for *B. pasteurii* growth than the other drilling fluids.

Growth Kinetics of *B. pasteurii* in a Drilling Fluid Composed of Two Materials. The growth kinetics of *B. pasteurii* in a drilling fluid composed of two materials is shown

https://doi.org/10.1021/acsomega.1c02616
ACS Omega 2021, 6, 25170−25178

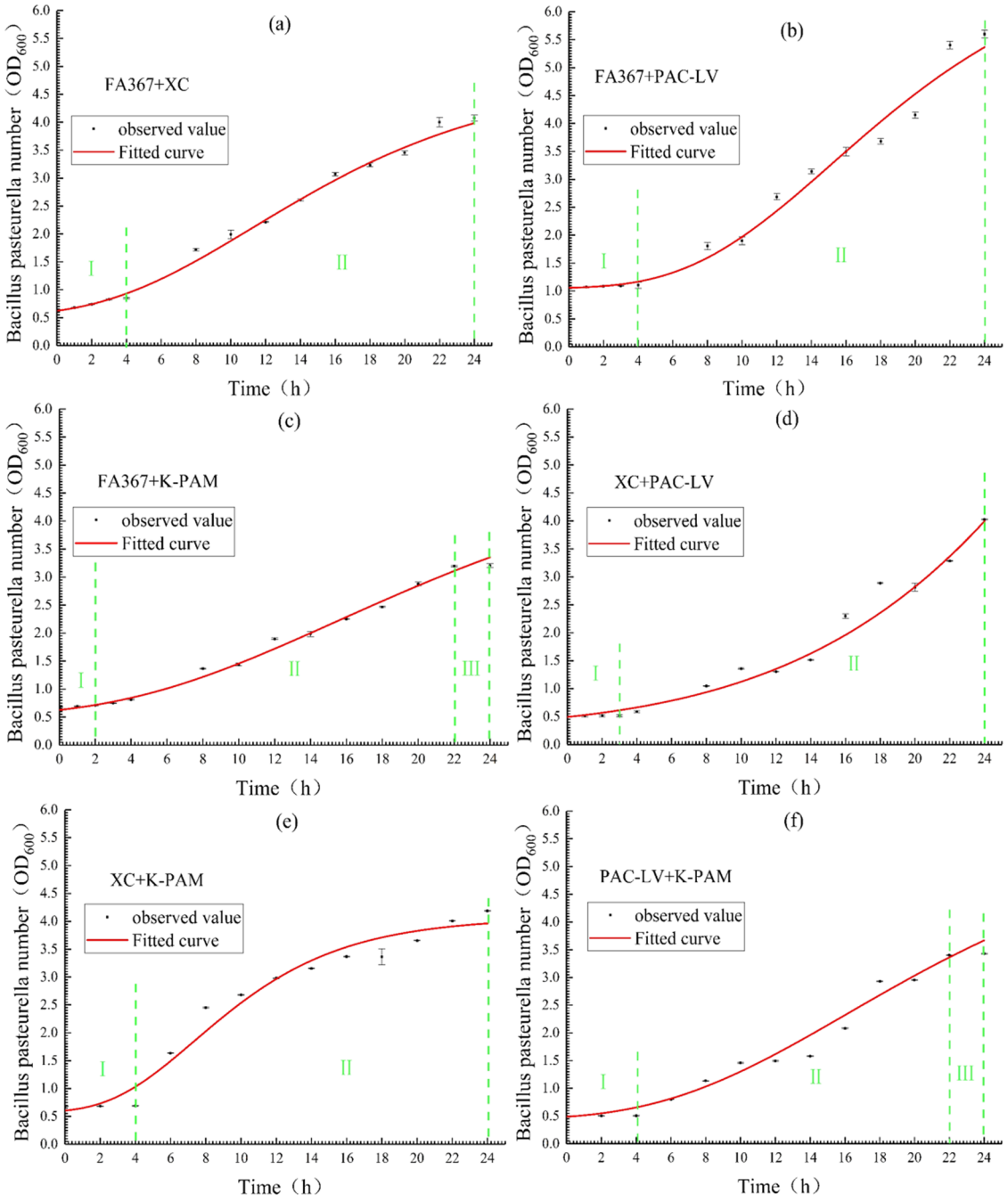

Figure 4. Growth curve of *B. pasteurii* in the drilling fluid containing (a) FA367 and XC; (b) FA367 and PAC-LV; (c) FA367 and K-PAM; (d) XC and PAC-LV; (e) XC and K-PAM; and (f) PAC-LV and K-PAM.

in Figure 4. In the six solid-phase drilling fluids, the growth lag period of *B. pasteurii* within 24 h was between 0 and 4 h. In the solid-free drilling fluid comprising FA367 and K-PAM, the lag time of *B. pasteurii* growth was the shortest at 2 h (Figure 4c).

In 24 h, *B. pasteurii* had the longest logarithmic phase in the solid-free drilling fluid composed of XC and PAC-LV, reaching 21 h, and the fitted growth curve showed a "concave up" shape, indicating that the growth of the bacteria was still in the log phase and considerably far away from reaching the stationary phase (Figure 4d). This is because both the constituent materials are polysaccharides; therefore, the drilling fluid composed of the two materials has more carbon sources and increased nutrient concentration, which is conducive to *B. pasteurii* growth. In the solid-free drilling fluid comprising PAC-LV and K-PAM, the growth logarithm period was the shortest at only 18 h (Figure 4f). In the other four solid-free drilling fluids, the growth logarithm period was 20 h.

Among all of the solid-free drilling fluids, *B. pasteurii* grew the best in the fluid composed of FA367 and PAC-LV, which had the highest OD_{600} value of 5.6. During the early logarithmic growth phase, the growth rate was high. However, in the later stages, the growth rate was decreased (Figure 4b). This is because PAC-LV is a type of anionic cellulose, a high-quality polysaccharide, and the pH value of the drilling fluid was moderate and suitable for *B. pasteurii* growth. However, *B. pasteurii* grew slowly after 22 h due to the presence of FA367, an amphoteric ion-coating agent, which binds to the anions in PAC-LV and reduces its water solubility. Among all of the

https://doi.org/10.1021/acsomega.1c02616
ACS Omega 2021, 6, 25170−25178

solid-free drilling fluids, *B. pasteurii* growth was the worst in the fluid composed of FA367 and K-PAM with an OD_{600} value of only 3.3, which might be related to the lack of additional nutrients in the drilling fluid.[26,27] Moreover, the pH of the drilling fluid was low, resulting in reduced bacterial growth and OD_{600} values (Figure 4c). Figure 4a–f shows that *B. pasteurii* growth rates in the drilling fluids composed of two materials were 14.308, 18.875, 10.521, 14.692, 14.608, and 12.200%, respectively.

The growth curves of *B. pasteurii* in the six drilling fluids were all S-shaped curves, consistent with the characteristics of the model used. The model fit and verification parameters are presented in Table 2.

Table 2. Model Fit and Verification Parameters (Drilling Fluid Composed of Two Materials)

drilling fluid composition	MSE	B_f	A_f
FA367 and XC	0.01420	0.98756	1.03595
FA367 and PAC-LV	0.06567	0.99151	1.05289
FA367 and K-PAM	0.01011	0.98836	1.04140
XC and PAC-LV	0.05048	0.99097	1.09239
XC and K-PAM	0.06080	1.01215	1.09347
PAC-LV and K-PAM	0.04045	1.03711	1.08962

Table 2 shows that the MSE after fitting the solid-free drilling fluid composed of FA367 and K-PAM was the smallest, whereas the MSE of the drilling fluid composed of FA367 and PAC-LV was the largest. However, the MSE values of all six types of solid-free drilling fluids were less than 0.1, indicating that the model fit appropriately. B_f and A_f of the six types of solid-free drilling fluids were close to 1. However, B_f was the closest to 1 in the solid-free drilling fluid composed of FA367 and PAC-LV, whereas A_f approached 1 in the solid-free drilling fluid composed of FA367 and XC.

Therefore, *B. pasteurii* had a short lag time, long logarithmic growth phase, and the most significant growth rate and highest concentration in the drilling fluid composed of XC and PAC-LV. Thus, this drilling fluid was considered the most suitable for *B. pasteurii* growth.

Growth Kinetics of *B. pasteurii* in a Drilling Fluid Composed of Three Materials. The growth kinetics of *B. pasteurii* in a drilling fluid composed of three materials is shown in Figure 5.

Within 24 h, in the solid-free drilling fluid composed of FA367, XC, and PAC-LV, the lag phase of *B. pasteurii* was the shortest at 3 h (Figure 5a). Among all of the solid-free drilling fluids, the fluid composed of FA367, PAC-LV, and K-PAM showed the longest growth lag period of 12 h (Figure 5c). In the other two solid-free drilling fluids, the growth delay period was 4 h (Figure 5b,d).

Among all of the solid-free drilling fluids, *B. pasteurii* grew the best in the fluid composed of FA367, PAC-LV, and K-PAM, with a maximum OD_{600} of 4.8. Because *B. pasteurii* is an

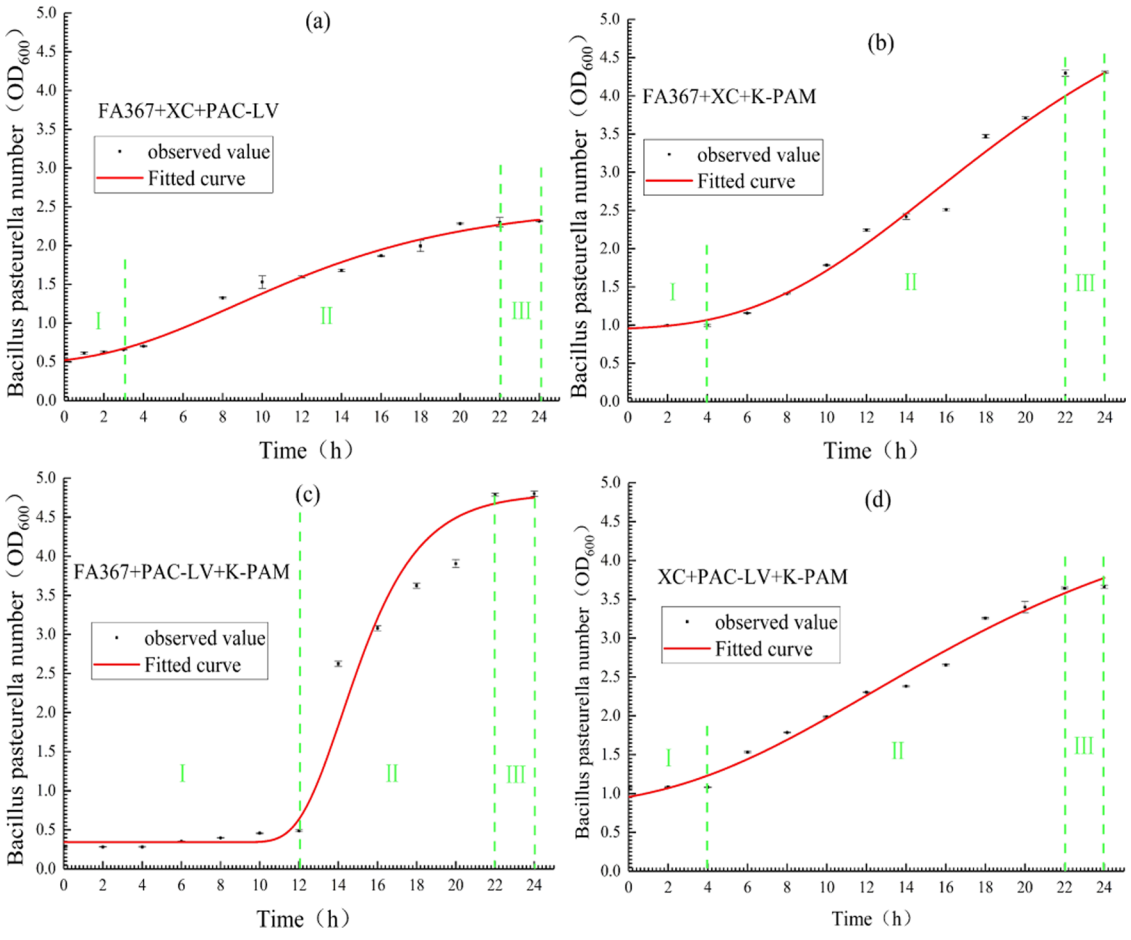

Figure 5. Growth curve of *B. pasteurii* in the drilling fluid containing (a) FA367, XC, and PAC-LV; (b) FA367, XC, and K-PAM; (c) FA367, PAC-LV, and K-PAM; and (d) XC, PAC-LV, and K-PAM.

https://doi.org/10.1021/acsomega.1c02616
ACS Omega 2021, 6, 25170−25178

alkalophilic bacterial strain that grows suitably in the pH range of 7.3−9, its growth rate increases with an increase in pH.[28−30] The pH value of this drilling fluid was high; therefore, it benefited *B. pasteurii* growth and increased its concentration. Among the solid-free drilling fluids, *B. pasteurii* growth was the worst in the fluid composed of FA367, XC, and PAC-LV, showing a maximum OD_{600} of 2.3 within 24 h (Figure 5a). This growth pattern was attributed to the pH value of the solid-free drilling fluid, which after mixing the three materials was less than 7—an acidic pH that does not benefit *B. pasteurii* growth. Figure 5a−d shows that *B. pasteurii* growth rates were 7.146, 13.804, 18.842, and 10.763%, respectively.

The growth curves of *B. pasteurii* in the drilling fluid composed of the three materials were all S-shaped curves, which was consistent with the characteristics of the used model. The model fit and verification parameters are presented in Table 3.

Table 3. Model Fit and Verification Parameters (Drilling Fluid Composed of Three Materials)

drilling fluid composition	MSE	B_f	A_f
FA367, XC and PAC-LV	0.00978	0.97741	1.05868
FA367, XC and K-PAM	0.02716	1.00166	1.04227
FA367, PAC-LV and K-PAM	0.12503	1.02114	1.15397
XC, PAC-LV and K-PAM	0.01608	0.99621	1.04728

Table 3 shows that the MSE value of the solid-free drilling fluid composed of FA367, PAC-LV, and K-PAM was close to 0.1, and the MSE values of the other three combinations of solid-free drilling fluids were less than 1. The MSE value was the lowest in the solid-free drilling fluid composed of FA367, XC, and PAC-LV. Therefore, for the solid-free drilling fluids composed of FA367, XC, and PAC-LV; FA367, XC, and K-PAM; and XC, PAC-LV, and K-PAM, the model fit well. B_f and A_f in the solid-free drilling fluid composed of FA367, XC, and K-PAM were the closest to 1, and the values of these factors of the solid-free drilling fluid composed of FA367, PAC-LV, and K-PAM deviated markedly from 1.

In summary, the solid-free drilling fluid composed of FA367, XC, and K-PAM was the most suitable for *B. pasteurii* growth because the growth lag time was short, the logarithmic growth period was long, the growth rate was significant, and high numbers were produced.

CONCLUSIONS

In the present study, four commonly used drilling fluid materials were selected and formulated into various drilling fluids. Using experimental and theoretical analyses, *B. pasteurii* growth in different drilling fluids was elucidated. The Gompertz model was used as a growth kinetics model to fit the experimental data. From the present study, we conclude the following:

(1) In different drilling fluids, *B. pasteurii* growth was significantly different. Among the drilling fluids tested in the present study, the suitable fluids (or combinations) for *B. pasteurii* growth were XC; XC and PAC-LV; and FA367, XC, and K-PAM.

Table 4. Composition and Performance of Drilling Fluids

number	composition	dosage (g/40 mL)	pH	funnel viscosity (s)	apparent viscosity (mPa·s)	plastic viscosity (mPa·s)
1	FA367	0.08	7.1	28	6	4
2	XC	0.1	8	25	11	10
3	PAC-LV	0.4	7.5	25	11	5
4	K-PAM	0.16	6.9	25	6	4
5	FA367	0.05	7.7	30	14	10
	XC	0.2				
6	FA367	0.05	8.1	28	8.5	7
	PAC-LV	0.2				
7	FA367	0.05	7.2	28	4.5	4
	K-PAM	0.05				
8	XC	0.05	7.7	30	10.5	8
	PAC-LV	0.2				
9	XC	0.05	7.4	25	6.5	6
	K-PAM	0.05				
10	PAC-LV	0.2	7.1	30	10.5	8
	K-PAM	0.05				
11	FA367	0.04	6.8	30	8.5	7
	XC	0.04				
	PAC-LV	0.04				
12	FA367	0.04	7.5	30	9	7
	XC	0.04				
	K-PAM	0.02				
13	FA367	0.04	7.6	28	7	5
	PAC-LV	0.04				
	K-PAM	0.04				
14	XC	0.04	7.2	29	9	7
	PAC-LV	0.02				
	K-PAM	0.04				

https://doi.org/10.1021/acsomega.1c02616
ACS Omega 2021, 6, 25170−25178

(2) The Gompertz model accurately predicted *B. pasteurii* growth in the different drilling fluids, and the prediction results were reliable. Hence, this model can also be used to predict *B. pasteurii* growth in other drilling fluids.
(3) The results of the present study provide a solid foundation for the development of microbial drilling fluid systems in the future.

MATERIALS AND METHODS

Materials. *Microbial Strain.* *B. pasteurii* DSM 33 was purchased from the China Microbial Species Inquiry Center.

Drilling Fluid Materials. Drilling fluid materials were divided into fluid loss agents, viscosity increasers, viscosity reducers, coating agents, and inhibitors. Four commonly used drilling fluid materials were selected: a strong zwitterionic coating agent (FA367) was purchased from Shandong Bright Chemical Products Co., Ltd.; a tackifier (biopolymer, XC) and a fluid loss agent (polyacrylate polymer, PAC-LV) were purchased from Tianjin Dingsheng Chemical Co., Ltd.; and an inhibitor (potassium polyacrylate, K-PAM) was purchased from Changzhou RunYang Chemical Co., Ltd.

Methods. *B. pasteurii Activation and Culture.* A liquid medium for *B. pasteurii* culture was prepared by mixing 5 g of sodium chloride (Xi'an Tianmao Chemical Co., Ltd.), 5 g of soy peptone, and 15 g of casein peptone (Zhengzhou All Stroke Chemical Products Co., Ltd.) in 1000 mL of deionized water (Jinan Joy Chemical Co., Ltd.). The pH of the solution was adjusted to 7.5 using NaOH (Xi'an Tianmao Chemical Co., Ltd.). Next, the solution was divided equally into 10 conical flasks of 250 mL capacity, sterilized in an autoclave at 1.05 MPa and 110 °C for 10 min, and cooled on a superclean worktable (produced by Suzhou Antai Air Technology Co., Ltd., model SW-CJ1FD) for subsequent use.

The activation steps were as follows:

(1) An ampoule bottle was wiped with absorbent cotton soaked in 75% alcohol, its top was heated with a flame, a small amount of sterile water was dropped onto the heated top to break it, and the top was knocked off the ruptured ampoule bottle using a file or pair of forceps.
(2) A sterile straw was used to suction by adding 0.1 mL of sterile water or the prepared liquid culture medium, which was subsequently placed in the bottle and left until the white bacterial powder in the ampoule had dissolved, and the lumps dissolved into suspension.
(3) The bacterial suspension in the liquid medium was suctioned and placed in a constant temperature shaking culture instrument (Shanghai Zhichu Instrument Co. Ltd., ZHTY-50s). The temperature was set to 30 °C, and the bacterial suspension was cultivated for 24 h at 200 r/min to obtain the bacterial liquid.

Preparation of Solid-Free Drilling Fluids. Depending on the drilling operation requirements, solid-free drilling fluids are generally composed of a single material or various materials in a specific proportion. To study the growth kinetics of *B. pasteurii* in solid-free drilling fluids, drilling fluid materials were prepared in three forms: single material, two-material combination, and three-material combination. Their combinations, dosages, rheological properties, and pH values are shown in Table 4.

In total, 40 mL of solid-free drilling fluid and 40 mL of sterilized liquid medium were mixed in an Erlenmeyer flask, and a pipette gun (Shanghai Yetuo Technology Co., Ltd.) was used to inject 20 mL into an Erlenmeyer flask. The conical flask was gently shaken to mix the liquid in the flask, and the mouth of the conical flask was sealed with medical gauze and incubated at 20 °C.

Microbial Quantity Detection. A UV2000 spectrophotometer (Shanghai Unico Instrument Co., Ltd.) was used to measure the concentration of the microorganisms. The photometer uses a light source to generate multiple wavelengths, and a light source of a specific wavelength is generated using a series of light-splitting devices. After the light source passes through the test sample, a part of the light source is absorbed. The absorbance value of the sample was calculated by comparing the difference in the absorbed light energy between the experimental and blank samples. The wavelength of the light used in the measurement in the present study was 600 nm, and the concentration of microorganisms was expressed as the OD_{600} value.

Kinetics Model. The four-parameter Gompertz model, also known as the modified Gompertz model, is a basic model of the pathogen modeling program and food microbiology model developed by the US Department of Agriculture and the Department of Agriculture, Fisheries and Food of the United Kingdom, respectively.[31−35] The expression is shown in eq 1 as follows

$$N_t = A + C \times \exp\left\{-\exp\left[2.718 \times \frac{\mu_{max}}{C} \times (\lambda - t) + 1\right]\right\} \quad (1)$$

where N_t is the number of microorganisms at time t, A is the asymptotic value that decreases infinitely with time (equivalent to the initial bacterial count), and C is the increment in the number of bacteria when the time increases indefinitely, that is, the difference between the initial number of bacteria and the maximum number of bacteria, μ_{max} is the maximum specific growth rate, and λ is the period of slow microbial growth.

In the present study, the MSE was used to evaluate the goodness-of-fit of the model. A small MSE value indicates that the predictive model for describing the experimental data is accurate.[36,37] The calculation formula is shown in eq 2 as follows

$$\mathrm{MSE} = \frac{1}{n}\sum_{n=1}^{N}(Y_n - y_n)^2 \quad (2)$$

where N is the number of data points, Y_n is the predictive value, and y_n is the observed value.

Model Validation. B_f and A_f are the most valuable model verification tools. The closer the value is to 1, the better is the prediction effect of the model.[38] The calculation formulas are shown in eqs 3 and 4 below

$$B_f = 10^{\sum_{i=1}^{n}\log(x_{predicted}/x_{observed})/n} \quad (3)$$

$$A_f = 10^{\sum_{i=1}^{n}\mathrm{I}\log(x_{predicted}/x_{observed})\mathrm{I}/n} \quad (4)$$

where B_f is the bias factor, A_f is the accuracy factor, n is the number of samples, $x_{predicted}$ is the model prediction, and $x_{observed}$ is the experimental measurement value.

AUTHOR INFORMATION

Corresponding Author

Zhijun Li − *College of Environment and Civil Engineering, Chengdu University of Technology, Chengdu, Sichuan*

https://doi.org/10.1021/acsomega.1c02616
ACS Omega 2021, 6, 25170−25178

610059, People's Republic of China; orcid.org/0000-0002-2550-1894; Email: lizhijun2014@cdut.edu.cn

Authors

Gan Zhao − *College of Environment and Civil Engineering, Chengdu University of Technology, Chengdu, Sichuan 610059, People's Republic of China*

Junxiu Chen − *College of Environment and Civil Engineering, Chengdu University of Technology, Chengdu, Sichuan 610059, People's Republic of China*

Kuo Liu − *College of Environment and Civil Engineering, Chengdu University of Technology, Chengdu, Sichuan 610059, People's Republic of China*

Haotian Xiang − *College of Environment and Civil Engineering, Chengdu University of Technology, Chengdu, Sichuan 610059, People's Republic of China*

Yu Tian − *College of Environment and Civil Engineering, Chengdu University of Technology, Chengdu, Sichuan 610059, People's Republic of China*

Complete contact information is available at: https://pubs.acs.org/10.1021/acsomega.1c02616

Notes

The authors declare no competing financial interest.

■ ACKNOWLEDGMENTS

This study was supported by the National Natural Science of China (Grant No. 41702388) and the Everest Technology Research Proposal of Chengdu University of Technology (Grant No. 80000-2020ZF11411).

■ REFERENCES

(1) Zheng, Y. Q.; Xia, D.; Li, B.; Weng, S. H.; Li, Y. Q. Application status and development trend of geological core drilling technology in resource exploration, *World. Nonferrous Metal*, 2019; pp 260−264.

(2) Wang, P. Q. Definition of the concept of fractured strata and thermodynamic analysis of breakage *J. Southwest Pet. Inst.* 1999, *211* 13 16.

(3) Hu, J. L.; Tao, S. X.; Ji, W. J. Discussion and practice of hole wall stabilization technology in fractured strata. *Drill. Eng.* **2011**, *38*, 30−32.

(4) Qi, C. The Hidden Trouble in the Process of Oil Drilling Construction and the Countermeasures. In *Science, Technology, Innovation Guide*; 2015; Vol. *12*, pp 176−177.

(5) Wang, L. C.; Wang, C. S.; Zhang, J. C. Study on mechanism analysis and method of borehole stability of scientific deep well. *Equip. Geotech. Eng.* **2019**, *20*, 25−28.

(6) Li, C.; Bai, Y.; Yu, Y.; Xu, X. C.; Fan, S.; Luo, P. Y. Stabilizing drilling fluid technology of fractured formation borehole wall in Shunbei Oilfield. *Drill. Fluid Completion Fluid* **2020**, *37*, 15−22.

(7) Zou, S. L.; Wang, C. S. Evaluation method and application of anti - collapse agent in fractured formation drilling fluid. *Oilfield Chem* **1999**, *04*, 3−5.

(8) Chen, X. P.; Li, S. G.; Yu, Y.; Zhou, d. Anti - sloughing drilling fluid technology of carbonate rock fracture formation in Shunbei oil and gas field. *Pet. Drill. Tech* **2020**, *48*, 12−16.

(9) Tao, S. X.; Li, X. D.; Wu, Z. M.; Huang, W. D.; Liu, F. D. Study and application of strong film forming wall-protection washing solution system. *Geol. Prospect.* **2014**, *50*, 1147−1154.

(10) DeJong, Jason T.; Fritzges, Michael B.; Nüsslein, Klaus. Microbially induced cementation to control sand response to undrained shear. *J. Geotech. Geoenviron. Eng.* **2006**, *132*, 1381−1392.

(11) Kantzas, A. *A Novel Method of Sand Consolidation Through Bacteriogenic Mineral Plugging*, Annual Technical Meeting, OnePetro, 1992; pp 46−52.

(12) Ferris, F. G.; Stehmeier, L. G.; Kantzas, A.; Mourits, F.M. Bacteriogenic Mineral Plugging. *J. Can. Pet. Technol.* **1997**, *36*, 56−59.

(13) Ramachandran, S. K.; Ramakrishnan, V.; Bang, S. S. "Remediation of concrete using micro-organisms". *ACI Mater. J.* **2001**, *98*, 3−9.

(14) Qian, C. X.; Wang, R. X.; Cheng, L.; Wang, J.Y. Theory of Microbial Carbonate Precipitation and Its Application in Restoration of Cement-based Materials Defects. *Chin. J. Chem.* **2010**, *28*, 847−857.

(15) Qian, C. X.; Wang, A. H.; Wang, H. Research progress of microorganism grouting for soil reinforcement. *Rock Soil Mech.* **2015**, *36*, 1537−1548.

(16) Tan, Y. F.; Xie, X. H.; Wu, T.; Wu, S. Q.; Lu, B. microscopic and mechanical properties of microorganism consolidation in sand. *Yellow River* **2017**, *39*, 112−116.

(17) Yu, Q. P.; Li, N.; Fu, P.; Wang, L. J.; Li, K. Experimental study on the effect of microorganism grouting on sand reinforcement. *J. China. Inst. WaterResour. Hydropower Res.* **2019**, *17*, 204−210.

(18) Chen, X. H.; Ma, Q.; Yang, Z.; Zhang, Z. C.; Li, M. Study on dynamic response of microorganism grouting for strengthening liquefied sand foundation. *Chin. J. Geotech. Eng.* **2013**, *35*, 1486−1495.

(19) Cai, H.; Xiao, J. Z.; Wang, Z. W.; Li, J. Experimental study on the solidification of silty soil based on MICP technology. *J. Geotech. Eng.* **2020**, *42*, 249−253.

(20) Bachmeier, Keri L.; Williams, Amy E.; Warmington, John R.; Bang, Sookie S. Urease activity in microbiologically-induced calcite precipitation. *J. Biotechnol.* **2002**, *93*, 171−181.

(21) De Muynck, Willem.; De Belie, Nele.; Verstraete, Willy. Microbial carbonate precipitation in construction materials: A review. *Ecol. Eng.* **2010**, *36*, 118−136.

(22) Grossi, Marco.; Parolin, Carola.; Vitali, Beatrice.; Riccò, Bruno1. Computer Vision Approach for the Determination of Microbial Concentration and Growth Kinetics Using a Low Cost Sensor System. *Sensors* **2019**, *19*, No. 5367.

(23) Qiang, C. X.; Wang, X.; Yu, X. N. Progress in research and application of microbe-al cement. *J. Mater. Eng. (Beijing, China)* **2015**, *43*, 92−103.

(24) Pei, D.; Liu, Z. M.; Hu, B. R.; Wu, W. J. Research progress on the mechanism and application of Bacillus pasteurii mineralization. *Prog. Biochem. Biophys.* **2020**, *47*, 467−482.

(25) Takahashi, N.; Fujita, Y.; Takahashi, N.; Nakamura, A.; Harada, T. Effect of xanthan gum-based food thickeners on the dissolution profile of fluoroquinolones oral formulations. *J. Pharm. Health Care Sci.* **2020**, *6*, No. 25.

(26) Achal, V.; Mukherjee, A.; Basu, P. C.; Reddy, M. S. Lactose mother liquor as an alternative nutrient source for microbial concrete production by Sporosarcina pasteurii. *J. Ind. Microbiol. Biotechnol.* **2009**, *36*, 433−438.

(27) Achal, V.; Mukherjee, A.; Reddy, M. S. ORIGINAL RESEARCH: Biocalcification by Sporosarcina pasteurii using corn steep liquor as the nutrient source. *Ind. Biotechnol.* **2010**, *6*, 170−174.

(28) Williams, S. L.; Kirisits, M. J. *Characterization of Live, Dead, Starved, and Heat-treated Sporosarcina Pasteurii Cells: Implications for Biomineralization in Construction Materials*, First International Conference on Bio-based Building Materials, RILEM Publications SARL, 2015; pp 324−330.

(29) Doyle, R. J. Bacterial Adhesion: Molecular and Ecological Diversity Wiley. *Trends Microbiol.* **1997**, *5*, 165−166.

(30) Martin, Derek.; Dodds, Kevin.; Ngwenya, Bryne T.; Butler, Ian B.; Elphick, Stephen C. Inhibition of Sporosarcina pasteurii under Anoxic Conditions: Implications for Subsurface Carbonate Precipitation and Remediation via Ureolysis. *Environ. Sci. Technol.* **2012**, *46*, 8351−8355.

(31) Dong, H. H.; He, L.; Lu, H. W.; Li, j. A microbial growth kinetics model driven by hybrid stochastic colored noises in the water environment. *Stochastic. Environ. Res. Risk Assess.* **2017**, *31*, 2047−2056.

(32) Saravanan, Pichiah.; Pakshirajan, K.; Saha, Prabirkumar. Growth kinetics of an indigenous mixed microbial consortium during

phenol degradation in a batch reactor. *Bioresour. Technol.* **2008**, *99*, 205−209.
(33) Feisther, V.A.; de Souza, A.A.U.; Trigueros, D.E.G.; de Mello, J.M.M.; de Oliveira, D.; Selene, M. A.; de Souza, G.U. Biodegradation kinetics of benzene, toluene and xylene compounds: microbial growth and evaluation of models. *Bioprocess Biosyst. Eng.* **2015**, *38*, 1233−1241.
(34) Feng, H. Y. Microbiological Prediction Model for Salmonella Growth and Sodium Hypochlorite Sterilization in Chicken at Different Temperatures. PhM Thesis, Zhejiang University, 2018.
(35) Lytou, Anastasia.; Panagou, Efstathios Z.; Nychas, George-John E. Development of a predictive model for the growth kinetics of aerobic microbial population on pomegranate marinated chicken breast fillets under isothermal and dynamic temperature conditions. *Food Microbiol.* **2016**, *55*, 25−31.
(36) Cotto, A.; Looper, J.K.; Mota, L.C.; Son, A. Quantitative Polymerase Chain Reaction for Microbial Growth Kinetics of Mixed Culture System. *J. Microbiol. Biotechnol.* **2015**, *25*, 1928−1935.
(37) Atungulu, G. G.; Thote, S.; Wilson, S. Storage of hybrid rough rice − Consideration of microbial growth kinetics and prediction models. *J. Stored Prod. Res.* **2016**, *69*, 235−244.
(38) Wei, Z. Y.; Yao, Y. K.; Pan, J. R.; Ye, H. M.; Lin, K.; Fang, T. Kinetic model of microbial growth in pasteurized milk. *J. Food Saf. Qual.* **2019**, *10*, 2311−2316.

https://doi.org/10.1021/acsomega.1c02616
ACS Omega 2021, 6, 25170−25178